Coupling between whistler waves and slow-mode solitary waves

A. Tenerani, F. Califano, F. Pegoraro, and O. Le Contel

Related Articles

Additional information on Phys. Plasmas

Coupling between whistler waves and slow-mode solitary waves

A. Tenerani,[1,2,a)] F. Califano,[2] F. Pegoraro,[2] and O. Le Contel[1]

[1]*LPP, CNRS/Ecole Polytechnique/UPMC, St. Maur-des-Fossés, France*
[2]*Physics Department, University of Pisa, Pisa, Italy*

The interplay between electron- and ion-scale phenomena is of general interest for both laboratory and space plasma physics. In this paper, we investigate the linear coupling between whistler waves and slow magnetosonic solitons through two-fluid numerical simulations. Whistler waves can be trapped in the presence of inhomogeneous external fields such as a density hump or hole where they can propagate for times much longer than their characteristic time scale, as shown by laboratory experiments and space measurements. Space measurements have detected whistler waves also in correspondence to magnetic holes, i.e., to density humps with magnetic field minima extending on ion-scales. This raises the interesting question of how ion-scale structures can couple to whistler waves. Slow magnetosonic solitons share some of the main features of a magnetic hole. Using the ducting properties of an inhomogeneous plasma as a guide, we present a numerical study of whistler waves that are trapped and transported inside propagating slow magnetosonic solitons. © 2012 American Institute of Physics. [http://dx.doi.org/10.1063/1.4717764]

I. INTRODUCTION AND AIMS

The study of the interplay between phenomena at ion and at electron dynamical scales is crucial in order to understand the physical mechanisms of basic plasma processes such as energy dissipation and particle acceleration and heating in space and laboratory plasmas. Presently, multi-point satellite measurements such as the Cluster satellites, by combining space and time measurements, make it possible to investigate simultaneously electron- and ion-scale phenomena and to inspect stationary and propagating magnetic and density structures.

An important example of coupling between ion- and electron-scales is provided by the correlation that has been found in space between whistler waves, which occur on the electron-scales, and magnetic field depressions associated to density humps that have typical scale lengths of the order of the ion-scales, usually interpreted as non-propagating mirror mode structures.[1–5] On the other hand, whistler waves can also interact with slowly propagating magnetohydrodynamic structures involving both density and magnetic field modulations. If the whistler waves become trapped inside such structures, the problem arises how low frequency nonlinear modes can act as carriers for higher frequency waves.

Whistler waves are electromagnetic right-handed polarized waves that propagate nearly parallel to the ambient magnetic field at frequencies in the range between the ion and the electron cyclotron frequency.[6] A known property of whistlers is that in the presence of plasma inhomogeneities, such as magnetic field aligned tubes of density enhancements or depletions, their energy can be guided for long times without being dispersed.[7–10] Examples of such ducted propagation has been found in satellite observations in the Earth's magnetosphere[11–13] and in laboratory plasmas.[14]

Magnetohydrodynamic waves also have been studied for decades both in space and laboratory plasmas. Recently, growing attention has been devoted to the study of oblique slow magnetosonic solitary waves, namely, of coherent structures at the ion-scale characterized by a density hump and a magnetic field depression.[15–18]

Despite many studies of both magnetosonic and whistler waves, their coupling has not been investigated in detail and is yet poorly understood. In this paper, we investigate the interaction between slow magnetosonic solitons and whistler waves by using a two-fluid model. Using the ducting properties of an inhomogeneous plasma as a guide, we propose a new mechanism of ducting and transport of whistler waves arising from a linear coupling with slow type magnetosonic solitons. Such a mechanism could explain spacecraft observations in the Earth's magnetosphere, namely, the recurrent detection of whistler waves correlated to magnetic holes.

This paper is organized as follows: in Sec. II, we present the two main problems of interest separately: the whistler waves trapping and the slow mode solitary wave. In Sec. II A, we treat the trapping of whistlers by an inhomogeneous magnetized plasma. The aim is to shed light on the ducting process using an equilibrium configuration simpler than the soliton solution. In this way, we can obtain quantitative conditions to be used to estimate the ducting conditions when the inhomogeneity is provided by the magnetosonic soliton. In Sec. II B, we introduce the slow mode solitary wave solutions of the two-fluid equations and discuss the role that these configurations can have in trapping whistler waves. In Sec. III, we describe the system of equations of the two-fluid model used in our simulations, the initial conditions, and the simulation parameters. In Sec. IV, we investigate the trapping of whistler waves by slow mode solitons numerically and present the results. Finally, conclusions are discussed in Section V.

a)Electronic mail: anna.tenerani@lpp.polytechnique.fr.

II. THEORETICAL BACKGROUND

A. Whistler wave trapping in magnetic and density ducts

It has been shown[7–10] that whistler waves propagating in a cold magnetized plasma in the presence of inhomogeneities axially symmetric and transverse to the ambient magnetic field of the plasma density can be channelled by these inhomogeneities (*density duct*). The variation of the index of refraction caused by the density inhomogeneity makes the wave trajectory bend such that the average propagation is along the duct direction. As a consequence, the wave becomes trapped by the duct.

In this section, we extend these results to the case where both the equilibrium plasma density and magnetic field are inhomogeneous in the plane perpendicular to the direction of the magnetic field.

The aim of this analysis is to study the problem of whistler wave trapping with a "simple" model. It will be used later as a reference for a more complex one, adopted in the numerical simulations, where the self consistent fields of the soliton are viewed by the whistler as perturbations of the ambient equilibrium. In order to mimic the configuration of interest (the slow mode soliton), we consider a plasma equilibrium characterized by a density hump and a magnetic field minimum, the *magnetic hole*.

Model—We want to study the trapping properties of the equilibrium magnetic field inhomogeneities in the framework of a fluid model. Therefore, we consider the regime $v_{th,e} \ll v_{ph}$ ($v_{th,e}$ and v_{ph} being the electron thermal velocity and the whistler phase velocity, respectively), and we use the cold dielectric tensor of a magnetized plasma, ε. This simplification is convenient because the cold dielectric tensor ε includes the basic effects of trapping, thanks to its dependence on the density and the magnetic field strength (through the electron cyclotron frequency ω_{ce}). Assuming, for the sake of illustration, a two dimensional spatial configuration and taking the gradients along the magnetic field lines to be negligible on the scale of the whistler wave length, the plasma can be represented in a slab geometry, with density and magnetic field gradients perpendicular to the magnetic field direction. For the sake of clarity, we define "magnetic hole" a fluid equilibrium with a density hump and a magnetic field depression perpendicular to the equilibrium magnetic field, as distinguished from a "density duct" that only has a perpendicular density inhomogeneity. This model allows us to highlight the basic mechanism of the whistler wave trapping and to obtain a quantitative estimate of the parameters to be used in the simulations, such as the value of the whistler frequency and the angle of propagation. We will show that a magnetic hole requires less strict conditions on the whistler wave parameters than a density duct in order to trap whistler waves.

Let us consider a bump-like density profile in the *x* direction, perpendicular to the background magnetic field $\mathbf{B}_y(x)$,
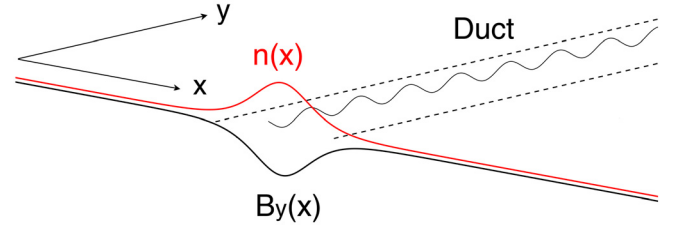

FIG. 1. Schematic representation of the trapping of whistler waves: the wave propagates in the plane (x, y) containing the magnetic field and the inhomogeneity direction and is localized inside the density hump. In the case of a warm plasma, a magnetic field depression of the form $B_y(x)$ is associated to the density enhancement.

which is taken to be directed along *y*. The background magnetic field has a minimum in correspondence to the density hump. A sketch of this configuration is illustrated in Fig. 1: the wave propagates in the (x, y) plane and is localized inside the magnetic hole. As shown in Ref. 8, the set of the two-fluid equations for a magnetized plasma can be arranged so as to obtain the following system of equations for the electric and magnetic fields, where a time dependence of the form $\exp(-i\omega t)$ has been assumed

$$\nabla(\nabla \cdot \mathbf{E}) - \nabla^2 \mathbf{E} = \frac{\omega^2}{c^2}(\varepsilon \cdot \mathbf{E}), \tag{1}$$

$$\nabla \cdot (\varepsilon \cdot \mathbf{E}) = 0, \tag{2}$$

$$\mathbf{B} = -i\frac{c}{\omega}\nabla \times \mathbf{E}. \tag{3}$$

Looking for spatial solutions of the form $A(x)\exp(ik_{\parallel}y)$, where $k_{\parallel} \equiv k_y$ is the parallel wave vector, Eq. (1) can be reduced to two coupled differential equations of second order for the electric field components E_x and E_z, while the third component E_y is obtained from Eq. (2). By rescaling the variable $w = x/L$, where L is the typical length of the large scale inhomogeneity such that $(c/\omega)/L \ll 1$, the two coupled equations for E_x and E_z can be solved by means of the WKB approximation.[8] We impose solutions of the form

$$A(w) = B(w)\exp\left(iL\omega/c\int^w q(w')dw'\right)$$

and retain only the terms to lowest order in $(c/\omega)/L$. Note that such a choice excludes the ducting mechanism described in Ref. 19 where the whistler energy propagates in the form of "surface waves" with frequency below the characteristic frequency of bulk whistler waves. The perpendicular wave vector $k_{\perp} \equiv (\omega/c)q = k_x$, for a given parallel wave vector $k_{\parallel}$ and frequency ω, must satisfy the whistler dispersion relation of a homogeneous plasma (in ion normalized units, see also Sec. III) obtained in the limit $\omega_{ci} < \omega < \omega_{ce} \ll \omega_{pe}$

$$k_{\perp,\pm}^2(x) = \frac{1}{2d_e^2(\omega/\omega_{ce}(x))^2}\left\{k_{\parallel}^2 d_e^2\left[1 - 2\left(\frac{\omega}{\omega_{ce}(x)}\right)^2\right] - 2n(x)\left(\frac{\omega}{\omega_{ce}(x)}\right)^2 \pm d_e k_{\parallel}\sqrt{d_e^2 k_{\parallel}^2 - 4n(x)\left(\frac{\omega}{\omega_{ce}(x)}\right)^2}\right\}. \tag{4}$$

Equation (4) corresponds to the whistler dispersion relation (see, for example, Ref. 20, Sec. 2.8) solved for the square of the perpendicular wave vector $k_\perp^2$, where $k_\perp^2 + k_\parallel^2 = k^2$. Note that, using ion normalized units, $d_e^2 = (m_e/m_p)$ and $\omega_{ce} = Bm_p/m_e$.

The whistler dispersion relation as expressed by Eq. (4) for the complex variable $k_\perp$ shows that, for fixed $k_\parallel$ and ω, there are two "branches" of the perpendicular wave vector corresponding to the plus and minus sign, respectively (the "upper" and the "lower" branch). For a solution given by a real $k_\perp$, we get a propagating whistler wave, while for an imaginary $k_\perp$, we get a purely evanescent (non propagating) whistler wave. The transition within a given branch from real to imaginary values is at the basis of the wave trapping and is determined by the local values of the density n and of the parameter ω/ω_{ce}.

The general WKB solution is given by a linear combination of the four wave solutions corresponding to the four possible wave vectors $\pm k_{\perp,\pm}$. Near the critical points, where $k_{\perp,\pm}^2 = 0$ or $k_{\perp,-}^2 = k_{\perp,+}^2$, the WKB approximation ceases to be valid. An analytical continuation of the solution in the complex x plane around these points is therefore necessary in order to extend the solution to all its domain of validity. The complex x plane is divided into different portions by the so called Stokes and anti-Stokes lines, which radiate out from the critical points.[21] When a Stokes line radiating from a turning point of a given branch is crossed, the two solutions of the given branch, say, the ones corresponding $+k_{\perp,-}$ and to $-k_{\perp,-}$, are coupled, corresponding to the reflection of a given wave when approaching a turning point. In an similar way, when a Stokes line radiating from a conversion point is crossed, the coupling between the two branches, for example, $+k_{\perp,+}$ and $+k_{\perp,-}$, occurs. The coupling between the two branches leads, for instance, to the leakage of a propagating wave, again approaching a turning point. Because of the coupling with the other branch at the conversion point, a fraction of the wave energy continues to propagate past the turning point.[8] The coefficients of reflection or conversion are exponentially small if the critical points are far from the real axis.

In this section, we consider only the trapping of whistler modes due to the presence of turning points on the real axis, where $k_{\perp,\pm}^2 = 0$. For simplicity, the conversion between different branches will be neglected here, assuming that the square root in Eq. (4) does not vanish on the real axis. Moreover, in order to look for solutions given by propagating waves or evanescent waves, we assume that $k_{\perp,\pm}^2$ is real, which means that the perpendicular wave vector is real (i.e., $k_{\perp,\pm}^2 > 0$) or imaginary (i.e., $k_{\perp,\pm}^2 < 0$). These assumptions correspond to the following condition:

$$k_\parallel^2 > \frac{4n(x)}{d_e^2}\left(\frac{\omega}{\omega_{ce}(x)}\right)^2. \qquad (5)$$

From Eqs. (4) and (5), it follows that the upper branch cannot be trapped in a magnetic hole (neither in a density duct). Indeed, $k_{\perp,+}^2$ is everywhere positive for frequencies $\omega/\omega_{ce} < 1/2$, and thus, the wave propagates in all regions. If $\omega/\omega_{ce} > 1/2$, then $k_{\perp,+}^2$ is positive when $k_\parallel^2 d_e^2 > n/[\omega_{ce}/\omega - 1]$. If this condition is satisfied inside the magnetic

hole, it is satisfied outside the magnetic hole as well, since $n(x)$ has lower values outside than inside the magnetic hole, and vice versa for the function $\omega_{ce}(x)$. Then, also in this range of frequencies, the wave propagates in all regions. We can therefore focus only on the lower branch $k_{\perp,-}$.

With the same reasoning as above, we see that the lower branch can be trapped in a magnetic hole (or in a density duct) only for frequencies $\omega/\omega_{ce} < 1/2$. Indeed, for frequencies $\omega/\omega_{ce} > 1/2$, the perpendicular wave vector corresponding to the lower branch is imaginary everywhere while for $\omega/\omega_{ce} < 1/2$, the perpendicular wave vector is real when

$$k_\parallel^2 < \frac{n/d_e^2}{\omega_{ce}/\omega - 1}, \qquad (6)$$

while it is imaginary when

$$k_\parallel^2 > \frac{n/d_e^2}{\omega_{ce}/\omega - 1}. \qquad (7)$$

To summarize, for frequencies $\omega/\omega_{ce} < 1/2$, trapping is possible in a magnetic hole (and in a density duct) if the parallel wave vector satisfies Eq. (5) everywhere (which means that $k_\perp$ is either imaginary or real), and satisfies Eq. (6) inside the magnetic hole, giving a propagating wave, and Eq. (7) outside the magnetic hole, giving an evanescent wave. Since we are interested in whistler modes trapped into the magnetic hole, from now on we consider only the lower branch in the frequency range $\omega/\omega_{ce} < 1/2$ and drop the subscript "−". For the sake of clarity we define n_{in} and n_{out} the density calculated at the center of the magnetic hole (thus in correspondence to the minimum of the magnetic field and to the density maximum) and outside the magnetic hole (where the medium is homogeneous), respectively. By analogy, we define the frequencies ω_{ce}^{in} and ω_{ce}^{out}, the electron cyclotron frequency calculated at the center and outside the magnetic hole, respectively. In this way, the trapping condition for the lower branch in a magnetic hole can be written as follows:

$$k_{inf} < k_\parallel < k_{sup}, \qquad (8)$$

where

$$k_{inf}(\omega) = \max\left\{\left[\frac{4n_{in}}{d_e^2}\left(\frac{\omega}{\omega_{ce}^{in}}\right)^2\right]^{1/2}, \left[\frac{n_{out}}{d_e^2}\frac{1}{\omega_{ce}^{out}/\omega - 1}\right]^{1/2}\right\} \qquad (9)$$

and

$$k_{sup}(\omega) = \sqrt{\frac{n_{in}}{d_e^2}\frac{1}{\omega_{ce}^{in}/\omega - 1}}. \qquad (10)$$

In Fig. 2, we show a graphical representation of the portions in the parameter space $(\omega/\omega_{ce}^{in}, k_\parallel)$ corresponding to real values of $k_\perp$, calculated at the center (solid lines) and outside (dashed lines) the channel provided by the magnetic hole or the density duct. Red and black lines correspond to the
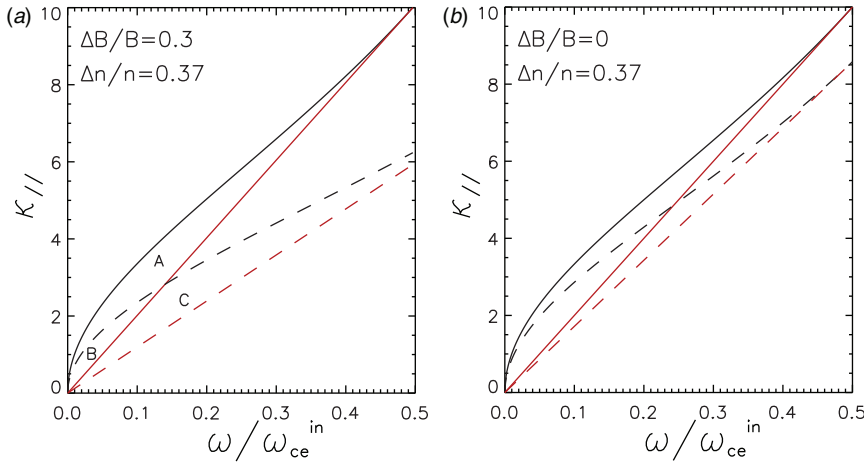
FIG. 2. Plot of the curves which bound the region in the parameter space $(\omega/\omega_{ce}^{in}, k_{\parallel})$ corresponding to real values of $k_{\perp,-}$. Solid and dashed lines are calculated in correspondence to the region inside and outside the channel, respectively. Red (straight) and black (curved) lines correspond to the right-hand-side of Eqs. (5) and (6), respectively. The portions a + b and b + c correspond to real values of $k_{\perp}$ inside and outside the inhomogeneous region, respectively. The portion "a" corresponds to the trapped modes. Left panel: plasma equilibrium with a magnetic hole; right panel: plasma equilibrium with a density hump on a uniform magnetic field.

right-hand-side of Eqs. (5) and (6), respectively. The left panel corresponds to a plasma equilibrium with a magnetic hole ($\Delta B/B = |B^{in} - B^{out}|/B^{out} = 0.3$ and $\Delta n/n = |n_{in} - n_{out}|/n_{out} = 0.37$) and the right panel to a density duct with the same density inhomogeneity than the magnetic hole ($\Delta B/B = 0$ and $\Delta n/n = 0.37$). Referring to Fig. 2, left panel, the points $(\omega/\omega_{ce}^{in}, k_{\parallel})$ lying in the portion a + b and b + c correspond to a propagating wave in the region inside and outside the channel, respectively. The intersection b of these two regions corresponds to the untrapped modes, as they propagate both inside and outside the channel. The trapped modes are those corresponding to the portion a, where $k_{\perp}$ is real inside and imaginary outside the channel. The maximum angle $\theta_{max}(\omega)$ of trapped modes for a given frequency is determined by k_{inf}, and by the corresponding $k_{\perp}(\omega, k_{inf})$

$$\theta_{max}(\omega) = \arctan\left[\frac{k_{\perp}(\omega, k_{inf})}{k_{inf}}\right]. \qquad (11)$$

A comparison between the magnetic hole, left panel in Fig. 2, and the density duct, right panel in Fig. 2, shows that the presence of magnetic variations (magnetic hole) leads to less strict trapping conditions. Indeed, for an equal density variation, the portion of trapped modes in a channel provided by both density and magnetic inhomogeneities is larger than in a channel formed only by a density inhomogeneity. In addition, the maximum angle of trapping (not shown here) results to be higher.

B. Slow magnetosonic solitons acting as carriers of whistler wave energy

We are interested in slow mode solitary waves because, as it will be explained in the following, they can trap whistler waves, similarly to magnetic holes. In addition, since solitary waves propagate almost unchanged, they provide an efficient channel that not only confines but also transports whistler energy at the typical soliton propagation speed.

Magnetosonic solitons are nonlinear one dimensional perturbations propagating in a warm plasma, obliquely to the equilibrium magnetic field.[15,18,22] Solitons are characterized by magnetic field and density perturbations in phase (fast

solitons) or in opposition of phase (slow solitons). Solitary waves propagate with a constant profile and arise when the nonlinear terms are balanced by the dispersion terms. In a two-fluid model, the required dispersion, which gives rise to magnetosonic solitons, is given by the Hall term and the electron inertia. Nonetheless, for non-perpendicular propagations, the Hall term dominates the dispersion and the typical scales of solitons are $\sim d_i$. It can be shown that at some level of approximation, the system of two-fluid equations can be reduced to a Korteweg-de Vries equation,[22] which has solitary wave solutions.

Let us consider a soliton moving in the positive x direction in a homogeneous magnetized plasma at rest, with equilibrium quantities defined as follows:

$$\mathbf{B} = \mathbf{B}_0 = (B_{0x}, B_{0y}, 0) \qquad \mathbf{u}_{i,e} = (0, 0, 0)$$

$$n = n_0 \qquad P_{i,e} = P_0,$$

where $\mathbf{u}_{i,e}$ and $P_{i,e}$ are the ion and electron velocity and pressure, respectively, n is the density, and $\mathbf{B}$ is the magnetic field. The angle of propagation of the soliton is defined as the angle between the direction of propagation, namely the x direction, and the equilibrium magnetic field $\mathbf{B}_0$. For future convenience, in order to define the soliton direction of propagation, we will use the angle φ_0, taken as the complementary angle to the angle of propagation, thus defined as $\varphi_0 = \arctan(B_{0x}/B_{0y})$. An explicit solitary solution of the two-fluid system of equations is obtained in Ref. 22 in the weakly nonlinear approximation. Both fast and slow solitons are found. Here we consider only the slow mode, as this mode has density and magnetic field in opposition of phase. The slow mode solitary solution depends on the amplitude of the perturbation A, on the angle φ_0, on the temperature and on the Alfvén speed which, in the homogeneous region, is equal to one in our units. The effects of the temperature enter through the sound speed c_s and the slow magnetosonic phase speed v_{p0}, and determines the velocity of propagation of the soliton and its width. Equations (12) and (13) represent the total magnetic field and the total density of the plasma, defined as the values of the homogeneous equilibrium plus the fluctuations associated to the soliton, $\mathbf{B}_{tot} = \mathbf{B}_0 + \mathbf{B}_{sol}, n_{tot} = n_0 + n_{sol}$

$$n_{tot} = 1 + n_{sol}, \quad B_{x,tot} = \sin\varphi_0,$$

$$B_{y,tot} = \cos\varphi_0 + \left[\frac{(v_{p0}^2 - c_s^2)}{\cos\varphi_0}\right] n_{sol}, \tag{12}$$

where

$$n_{sol} \propto \frac{A}{\cos h^2\left[\sqrt{\frac{A}{12\mu(\varphi_0,P_0)}}x\right]}. \tag{13}$$

The other plasma quantities are given explicitly in Appendix A, including the expression for the function $\mu(\varphi_0, P_0)$. Quantities are normalized to asymptotic equilibrium values outside the soliton.

According to this theoretical analysis, the propagation speed of the soliton is $V_0 = v_{p0} + A/3$ and the typical width is $\ell \sim 2\sqrt{12\mu/A}$. The function μ, which determines the width of the soliton, is a growing function of the temperature, ranging from values smaller than, or of the order of, d_i to values much greater than d_i. Note that for the slow mode $v_{p0} < c_s$. Thus, from the last of Eqs. (12), which defines B_y^{tot}, it follows that the magnetic field perturbation is in opposition of phase with the density perturbation. The analytical solution for the slow soliton is valid as long as the propagation is not parallel ($\varphi_0 = \pi/2$) in which case μ equals zero (if $c_s < 1$) or infinity (if $c_s > 1$).[22]

To summarize, the main features of slow mode solitons are as follows: they carry a density hump perturbation associated to a magnetic field depletion and propagate obliquely with respect to the background equilibrium magnetic field at speeds, which are much smaller than that of whistler waves (greater than unity). This inhomogeneous system, which can be represented by an oblique solitary perturbation moving in a homogeneous plasma at rest, is more complicated than the magnetic hole discussed previously, which instead has purely perpendicular gradients with respect to the magnetic field. Nevertheless, as a first approximation, it is possible to consider the soliton perturbation superposed to the background equilibrium as a local and instantaneous magnetic hole for whistlers that are injected inside the soliton.

III. MODEL EQUATIONS, INITIAL CONDITIONS, AND PARAMETERS

In order to describe numerically the trapping and transport of whistlers by solitary waves in a magnetized plasma, we use a quasi neutral adiabatic two-fluid model. The set of equations for ions and electrons, with labels i and e, respectively, are normalized using as characteristic quantities the ion mass density nm_i, the Alfvén velocity $v_a = B/\sqrt{4\pi nm_i}$, and the collisionless ion skin depth $d_i = c/\omega_{pi}$. With this choice $d_e^2 = m_e/m_i$ and $\omega_{ce} = B/d_e^2$. The two-fluid model equations, in dimensionless form, are

$$\partial n/\partial t + \nabla\cdot(n\mathbf{U}) = 0, \tag{14}$$

$$\partial\mathcal{S}_{e,i}/\partial t + \nabla\cdot(\mathcal{S}_{e,i}\mathbf{u}_{e,i}) = 0, \quad \mathcal{S}_{e,i} = P_{e,i}n^{1-\Gamma}, \tag{15}$$

$$\partial(n\mathbf{U})/\partial t = -\nabla\cdot[n(\mathbf{u}_i\mathbf{u}_i + d_e^2\mathbf{u}_e\mathbf{u}_e) + (P_e + P_i + B^2/2 - \mathbf{BB})], \tag{16}$$

$$(1 - d_e^2\nabla^2)\mathbf{E} = -\mathbf{u}_e\times\mathbf{B} - (1/n)\nabla P_e$$
$$- d_e^2\{\mathbf{u}_i\times\mathbf{B} - (1/n)\nabla P_i + (1/n)$$
$$\nabla\cdot[n(\mathbf{u_i}\mathbf{u_i} - \mathbf{u_e}\mathbf{u_e})]\}, \tag{17}$$

$$\mathbf{u_e} = \mathbf{U} - \mathbf{j}/n, \quad \mathbf{u}_i = \mathbf{U} + d_e^2\mathbf{j}/n, \quad \mathbf{U} = \mathbf{u}_i + d_e^2\mathbf{u}_e, \tag{18}$$

$$\nabla\times\mathbf{E} = -\partial\mathbf{B}/\partial t, \quad \mathbf{j} = \nabla\times\mathbf{B} + \hat{\mathbf{z}}j_z^{ext}. \tag{19}$$

In these equations, $\mathbf{E}$ and $\mathbf{B}$ are the electric and magnetic field, $\mathbf{u}_{i,e}$ is the ion (or electron) velocity, $\mathbf{j}$ is the current, $j_z^{ext}\hat{\mathbf{z}}$ is an external forcing current used to inject whistlers, $P_{i,e}$ is the pressure of ions and electrons, and Γ is the adiabatic index. The equations above are obtained by combining the ion and electron fluid equations. In particular, the generalized Ohm's law, given by Eq. (17), is obtained by subtracting the electron momentum equation from the ion momentum equation and we assumed constant density $n \sim 1$ in the electron inertia term on the left hand side.[23]

The dimensions of the simulation box, L_x and L_y, and the resolution of the grid, dx and dy, are chosen in order to find a compromise between the different time and length scales at play. L_y is chosen in order to let the whistler wave train propagate for several tens of ω_{ci}^{-1}, without reaching the boundaries. L_x is chosen in order to contain the soliton, which is wider or of the order of d_i and moves at a speed $V \sim 0.1$. Finally, the mesh size must resolve the whistler wavelength. In Table I, we report the parameters of the simulation box. The ion to electron mass ratio is fixed to $m_p/m_e = 100$.

As initial condition, we consider a slow mode solitary wave centered in the simulation domain and superposed to a homogeneous magnetized plasma at rest. Oblique whistlers, as explained in the following, are injected artificially in the simulation box, during the initial phase, in correspondence to the soliton. In order to do this, we make use of an oscillating forcing current lasting over a characteristic time τ. In Fig. 3, we show a schematic view of the system. The dashed lines indicate the region filled by the soliton moving in the positive x direction with velocity V; $\mathbf{B}_{tot}^{in}$ is the total magnetic field at the center of the soliton, forming an angle φ with the y axis, and $\mathbf{k}$ is the whistler wave vector. In particular, when

TABLE I. Parameters of the injected whistler mode, of the simulation box and the characteristic width of the soliton ℓ.

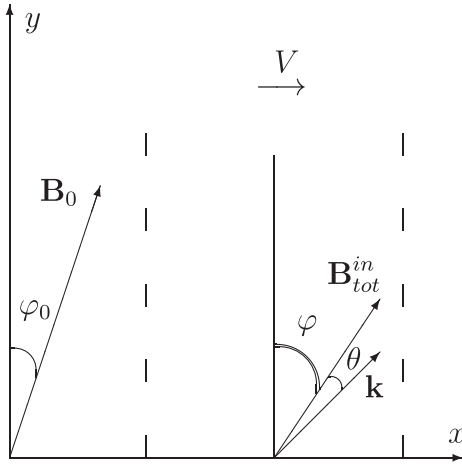|	ω_0	$\omega_0/\omega_{ce}^{in}$	θ	L_x	L_y	dx	dy	ℓ
Sim. 1	2.37	0.03	−0.198	24π	160π	0.08	0.1	2
Sim. 2	2.37	0.03	0.6	24π	60π	0.08	0.04	2
Sim. 3	2.37	0.03	1.25	24π	60π	0.08	0.04	2
Sim. 4	8	0.1	−0.198	24π	60π	0.08	0.04	2
Sim. 5	8	0.1	0.6	24π	60π	0.08	0.04	2
Sim. 6	8	0.1	1.3	24π	60π	0.08	0.04	2
Sim. 7	3	0.04	−0.24	24π	160π	0.08	0.1	13
Sim. 8	3	0.04	0.3	24π	120π	0.08	0.08	13
Sim. 9	3	0.04	0.6	24π	240π	0.08	0.16	13

FIG. 3. Schematic view of the system. The dashed lines indicate the region filled by the soliton moving in the positive x direction with velocity V; $\mathbf{B}_{tot}^{in}$ is the total magnetic field at the center of the soliton, forming an angle φ with the y axis, and $\mathbf{k}$ is the whistler wave vector, which forms an angle θ with the magnetic field $\mathbf{B}_{tot}^{in}$. Outside the soliton, the equilibrium magnetic field $\mathbf{B}_0$ forms an angle φ_0 with the y axis.

TABLE II. Parameters of the solitons.

	A	$P_{0i,e}$	φ_0	ℓ	$B_{y,tot}^{in}$	n_{tot}^{in}	φ	V	ω_{ce}^{in}
Sim. 1–6	0.073	0.05	0.17	~ 2	0.847	1.873	0.198	0.09	86.4
Sim. 7–9	0.035	0.5	0.17	~ 13	0.694	1.181	0.240	0.12	71.4

unchanged their initial profile over times $t \sim 1000$, until they exit from the simulation box.

In Fig. 4, we show two examples of quasi perpendicular ($\varphi_0 = 0.17$) magnetosonic solitons propagating along the x axis at three different times up to $t \sim 1000$. The red lines represent the density profile n_{tot} and the black lines the magnetic field $B_{y,tot}$. In the left panel, we represent a narrow, strong amplitude soliton ($\Delta n/n \sim 0.9$) and in the right panel a wider and weaker soliton ($\Delta n/n \sim 0.2$). Notice that the initial soliton profile slightly modify during the temporal evolution, especially for large amplitude solitons, since the analytical profile is not an exact solution of the two-fluid system. For the sake of clarity, we indicate with a subscript "tot" the quantities resulting from the sum of the homogeneous background equilibrium plus the soliton perturbations. These large scale variation fields can be considered as the "inhomogeneous equilibrium" supporting the whistler waves.

Finally, we generate small amplitude oblique whistlers with frequency ω_0 and propagating at an angle θ with respect to the *total* magnetic field direction with an external forcing current. The external forcing is spatially confined inside the soliton and is applied during a characteristic time scale τ by means of a current along the z axis, J_z^{ext} (see Eq. (19)), given by

$$J_z^{ext}(x,y,t) \propto e^{-(y'/\ell_y^J)^2} e^{-(x'/\ell_x^J)^2} e^{-t/\tau} \cos(\omega_0 t), \quad (20)$$

where x' and y' are defined as follows:

$$x' = x\cos(\theta + \varphi) - y\sin(\theta + \varphi),$$

$$y' = x\sin(\theta + \varphi) + y\cos(\theta + \varphi).$$

The length scales ℓ_y^J and ℓ_x^J satisfy $\ell_y^J \ll \ell_x^J$ and ℓ_x^J is of the order of the width of the soliton. Moreover, $\ell_x^J k_{y'} \gtrsim 1$, where $k_{y'}$ is the wave vector of whistlers along the rotated direction

whistlers are generated inside the soliton, the subscripts "$\perp$" and "$\parallel$" of the wave vector refer to the total magnetic field $\mathbf{B}_{tot}^{in}$ at the center of the soliton. Outside the soliton, the total magnetic field reduces to the equilibrium magnetic field $\mathbf{B}_0$, forming an angle φ_0 with the y axis.

The analytical form of the fields representing the soliton superposed to the homogeneous equilibrium at the initial time is given in Appendix A. The parameters of the soliton, listed in Table II, are chosen in order to have a narrow soliton with a width ℓ of the order of the ion skin depth (simulations 1 to 6) or a wider soliton with ℓ of the order of several ion skin depths (simulations 7 to 9).

To our knowledge, the numerical stability of the approximate solutions discussed in Sec. II has never been investigated. Therefore, before considering the full problem including the injection of the whistlers, we tested the stability of the soliton solutions numerically. Our results show that they are well stable in the range of propagation angles $\varphi_0 = 0.57 - 0.17$ and of typical variations with respect to the equilibrium $n_{sol} \sim 0.02 - 0.8$, $|B_{y,sol}|/B_{0y} \sim 0.01 - 0.5$. They propagate at the expected velocity maintaining almost
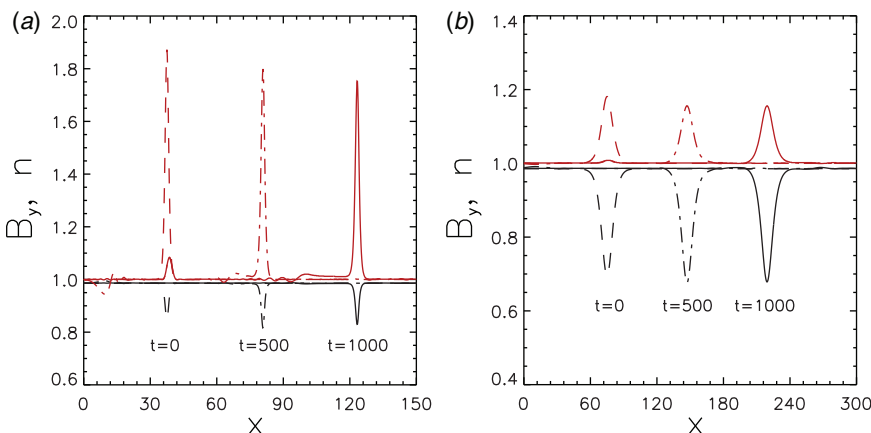

FIG. 4. Examples of slow magnetosonic solitons at three different times: the black lines (depletions) represent the magnetic field $B_{y,tot}$ and the red lines (humps) the density n_{tot}. In the left panel we represent a narrow, strong amplitude soliton ($\Delta n/n \sim 0.9$) and in the right panel a wider and weaker soliton ($\Delta n/n \sim 0.2$). Notice that the initial soliton profile slightly modify during the temporal evolution, especially for large amplitude solitons, since the analytical profile implemented as initial condition is not an exact solution of the two-fluid system.

y', so that we can inject inside the soliton almost plane waves. The injected whistlers have indeed wave vectors within a narrow cone centered in correspondence with the mode that we expect according to the chosen values of frequency ω_0 and angle θ. The parameters of the forcing and thus of the injected whistlers, listed in Table I, are chosen making use of the trapping conditions discussed in Sec. II A. In particular, we use as reference the maximum trapping angle defined by Eq. (11). The maximum angle of trapping at a given frequency ω_0, that we define as $\theta_{max}^{\omega_0}$, allows us to choose the frequency ω_0 and the angle θ properly in order to inject a specified whistler mode that we expect to be trapped or not.

IV. TRAPPING OF WHISTLER WAVES BY SLOW MAGNETOSONIC SOLITONS: NUMERICAL RESULTS

In this section, we show, by means of numerical simulations, that whistlers can be trapped and transported away by a slow magnetosonic soliton. Even if a slow soliton propagating in a homogeneous magnetized plasma is more complicated than the so called magnetic hole, as a first approximation the same properties of whistler ducting apply, and the trapping conditions found for the magnetic hole discussed in Sec. II A are therefore a good reference when asking which whistler modes can be trapped by the soliton.

We have investigated the slow magnetosonic ducted and unducted regime of whistler modes by varying the typical width of the soliton. Here, we report two different typical cases: a narrow soliton of width $\ell \sim 2 \lesssim k^{-1}$ and a wider soliton of width $\ell \sim 13 > k^{-1}$ (in units of d_i), where k is the whistler wave vector estimated for a given frequency and propagation angle from the two-fluid cold dispersion relation (see Eq. (B1) in Appendix B). A list of the parameters used in the simulations for the "small" and "large" soliton is listed in Table II. The wider soliton has a weaker density hump but a stronger magnetic field depression than the narrow one. The injected whistler modes fluctuate at low frequencies ($\omega_0 \ll 0.1\omega_{ce}^{in}$) or high frequencies ($\omega_0 \sim 0.1\omega_{ce}^{in}$) with different angles of propagation ranging from $\theta \ll \theta_{max}^{\omega_0}$ to

$\theta > \theta_{max}^{\omega_0}$. In the following, we focus on two simulations, namely, Sim. 1 for the narrow soliton and Sim. 7 for the wide soliton, to show the trapping of whistlers.

In these simulations, the injected whistlers have frequency $\omega_0 \sim 0.03\,\omega_{ce}^{in}$ and $\omega_0 \sim 0.04\,\omega_{ce}^{in}$, respectively. They are injected along the y axis, slightly oblique with respect to the local total magnetic field, forming an angle $\theta = -0.198$ and $\theta = -0.24$, respectively, then satisfying $|\theta| \ll \theta_{max}^{\omega_0}$. The forcing current oscillates at the center of the simulation domain and switches off exponentially on a characteristic time shorter with respect to that of the soliton propagation. In this way, the forcing generates two finite size wave packets in the (x,y) plane propagating away from the source region in the two opposite directions, namely, in the positive y direction (upward) and in the negative y direction (downward). The two wave packets propagate upward or downward, respectively, and remain spatially confined along the inhomogeneous x direction in correspondence to the soliton, following its displacement along x. This is shown in Fig. 5 by the contour plots of the x component of the magnetic field b_x of the whistler waves in the simulation domain when the current has switched off and the wave packets are well developed. The profile of the soliton is represented (not in scale) by black lines, and the dashed line corresponds to the soliton at time $t = 0$. The left panel represents the two wave packets at time $t = 100$, for the narrow soliton. In the middle panel, we show the propagation of the same wave packets as injected in Sim. 1, but in a homogeneous equilibrium, i.e., with $B_{0y} = B_{y,tot}^{in} = 0.847$ and $n_0 = n_{tot}^{in} = 1.873$. We see that in the absence of the soliton, the injected wave packets spread out during propagation. Finally, the right panel shows the wave packets at time $t = 60$, for the wide soliton. To summarize, our simulations provide evidence that the waves, initially injected inside the soliton structures, propagate along the duct provided by the soliton, upward or downward, advected at the same time in the perpendicular x direction by the soliton. The whistlers are thus confined and transported by the slow soliton over times much larger than their typical time scale.
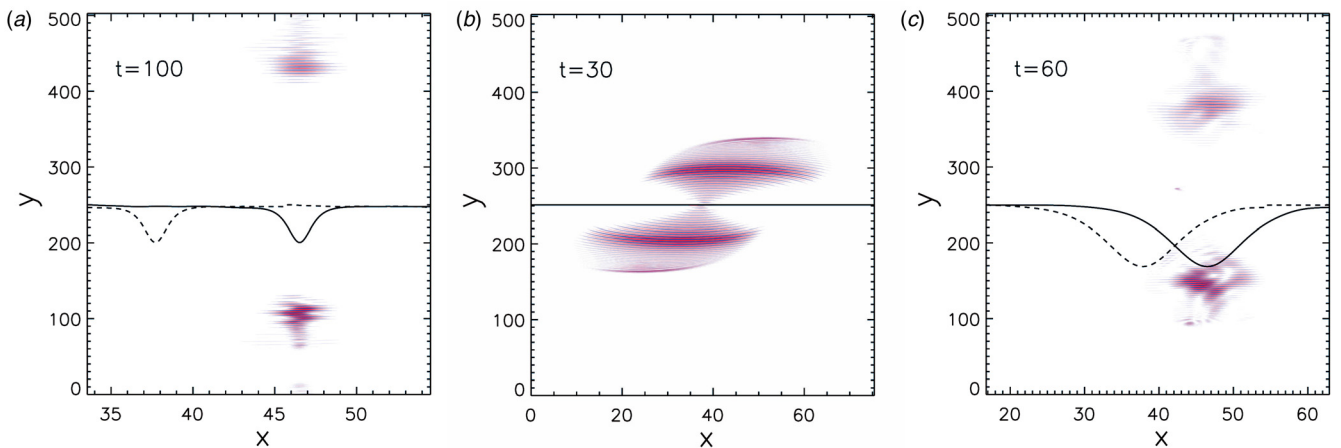

FIG. 5. Contour plot of the x component of the whistler magnetic field b_x. The profile of the soliton is represented by the black lines. The dashed line represents the soliton at time $t = 0$. Left panel: trapping of whistlers in Sim. 1 at time $t = 100$. Middle panel: the whistler wave packets in the entire space domain at $t = 30$ as in Sim. 1 but in the absence of the soliton. Right panel: trapping of whistlers in Sim. 7 at time $t = 60$. Notice that in these and in the following pictures, the length scales along the x and y axes are different.
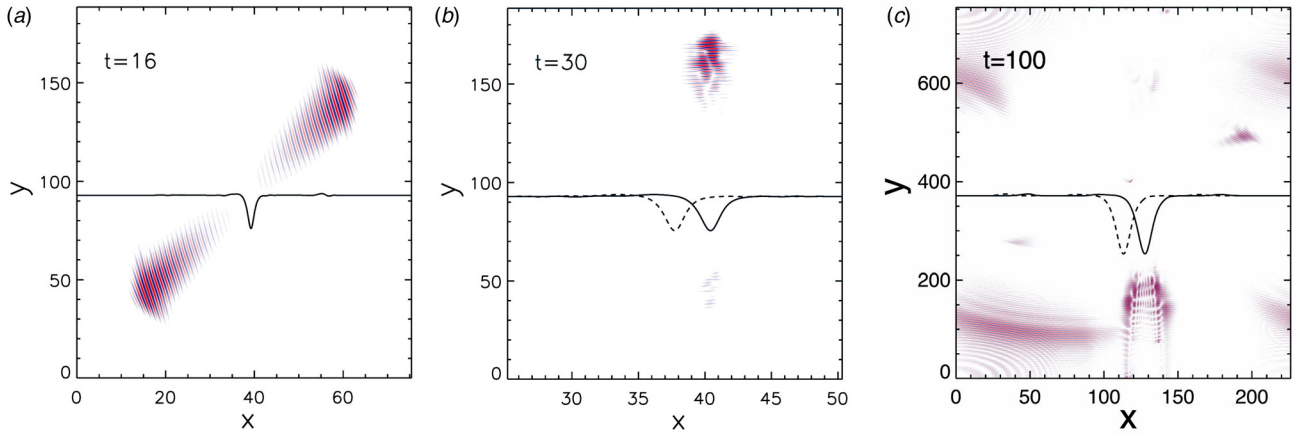
FIG. 6. Contour plot of the x component of the whistler magnetic field b_x, with the profile of the soliton represented by the black lines. The dashed line corresponds to the soliton at $t = 0$. Left panel: Sim. 6 at time $t = 16$, corresponding to a high frequency, highly oblique whistler that escapes from the narrow soliton. Middle panel: Sim. 4 at time $t = 30$, corresponding to a high frequency whistler that is trapped only in the upward direction while the downward wave packet becomes evanescent after one reflection. Right panel: Sim. 9 at time $t = 60$, corresponding to an upward whistler that escapes outside the soliton while the downward wave packet is trapped. The periodic boundary conditions cause the waves approaching the upper (lower) boundary of the simulation box to appear in the lower (upper) boundary.

We consider now two simulations, Sim. 3 and Sim. 6 where we inject highly oblique whistlers with $\theta > \theta_{max}^{\omega_0}$. In this case, the waves escape outside the solitons. An example is shown in Fig. 6, left panel, where we show the contour of b_x and the profile of the soliton at time $t = 16$ in the case of Sim. 6. Here, the injected whistlers are at high frequency ($\omega_0 \sim 0.1 \omega_{ce}^{in}$) and at an angle of propagation $\theta = 1.3$.

These results are in good agreement with the ducting theory. However, the model used in our numerical study is far richer than the reference model of the magnetic hole (Sec. II A), and there are important effects that can modify the trapping conditions.

First of all, even if we neglect the displacement of the soliton, there is a finite perturbation in the plasma velocity of the form $\mathbf{U}(x)$ (see Eqs. (A4) and (A5) in Appendix A). The presence of the fluid velocity introduces an asymmetry in the system, due to the Doppler effect, between wave packets propagating upward and downward, $k_y > 0$ and $k_y < 0$, respectively. Second, there are gradients along the total magnetic field, which can drive whistlers outside the soliton even if trapping conditions are satisfied. In the case of the magnetic hole, $k_\parallel$ and ω are fixed quantities, while for the soliton ω and k_y are constant, but the parallel wave vector varies as the whistler propagates inside the soliton. As a consequence, while the whistler propagates towards the edge of the soliton, $k_\parallel$ can approach the value k_{inf} (as defined in Sec. II A, see also Fig. 2, left panel), thus allowing the whistler to become untrapped. An example is given in Fig. 6, right panel, which refers to Sim. 9. In this simulation, only the lower wave packet is trapped while the upper wave packet is guided outside the soliton. An interpretation of Sim. 9 can be given in terms of geometrical optics. Since the soliton moves along the x axis at a speed $V \sim 0.1$ much smaller than the whistler phase velocity (greater than unity), as a first approximation, we neglect the displacement of the soliton. Because of the Doppler shift, the frequency ω_0 measured in the simulation is given by

$$\omega_0(\mathbf{k}, x) = \omega(\mathbf{k}, x) + \mathbf{k} \cdot \mathbf{U}(x), \tag{21}$$

where $\omega(\mathbf{k}, x)$ is the whistler two-fluid dispersion relation in a plasma at rest obtained in the cold limit (see Eq. (B1) in Appendix B). The dispersion relation $\omega(\mathbf{k}, x)$ is given in terms of k_y and k_x and the density and magnetic field profiles are given by $n = 1 + n_{sol}$ and $\mathbf{B} = \mathbf{B}_0 + \mathbf{B}_{sol}$, respectively. In the framework of the geometrical optics, the contours of ω_0 in the plane (k_x, x) for fixed k_y represent the orbits of the whistler wave packet. The solution of the Hamiltonian system

$$\frac{\partial \omega}{\partial x} = -\dot{k}_x(t), \qquad \frac{\partial \omega}{\partial k_x} = \dot{x}(t)$$

gives the evolution of the wave vector and the trajectory of the wave packet. In Fig. 7, we show the contours of ω_0 as defined in Eq. (21) obtained using the soliton profile of Sim. 9. The wave vector k_y can be estimated from the forcing frequency and injection angle taking into account the Doppler shift, giving $k_y \sim 1.3$ and $k_y \sim -1.7$. The contours in Fig. 7 show that the orbit corresponding to $\omega_0 = 3$ is open for the wave packet propagating upward while it is closed for the wave packet propagating downward. A Fourier analysis of the x component of the magnetic field in Sim. 9 confirms that the wave vectors with $|k_y| \sim 1.7$ are trapped inside the soliton. Similar results are obtained for Sim. 2 and Sim. 8.

However, because of the movement along the x axis, the soliton behaves as a "moving mirror," thus causing the frequency of the injected whistler to change with time. We qualitatively estimate the shifted frequency after the first reflection at the soliton edge $\omega_0' = \omega_0 - 2\mathbf{k} \cdot \mathbf{V}$. The change in frequency could cause the wave to become evanescent. An example is given by Sims. 4 and 5 in a high frequency whistler regime ($\omega \sim 0.1 \, \omega_{ce}^{in}$) and using a narrow soliton. In these simulations, only the upper wave packet is trapped, as expected, while after the first reflection at the left boundary of the soliton, the lower wave packet becomes evanescent.
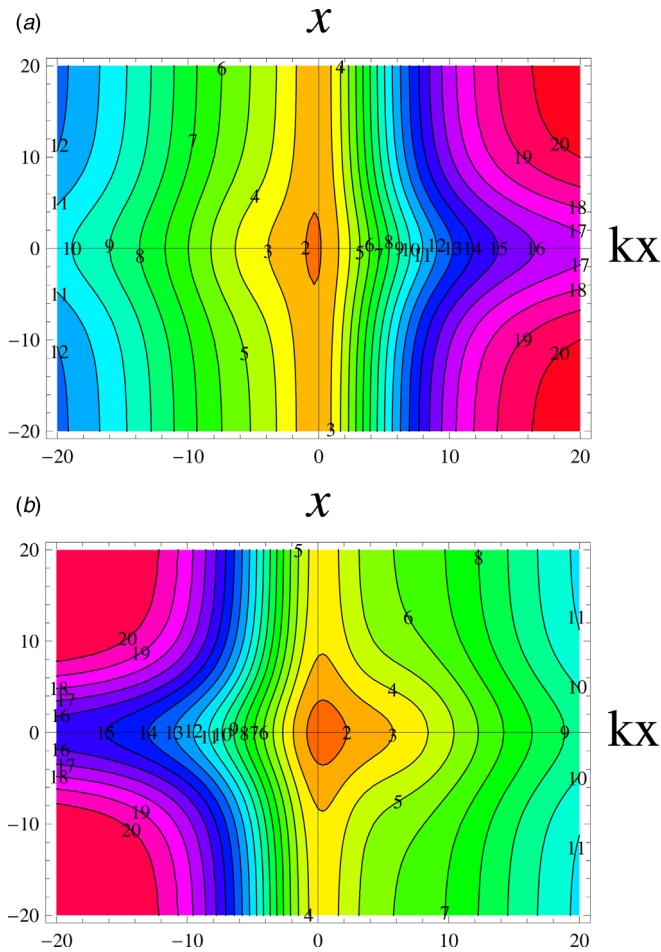
FIG. 7. Contours of the whistler dispersion relation in the rest frame of the soliton, $\omega_0(\mathbf{k}, x) = \omega(\mathbf{k}, x) + \mathbf{k} \cdot \mathbf{U}(\mathbf{x})$, in the (k_x, x) plane with the parameters of Sim. 9. The upper panel refers to the upward wave packet, which has $k_y \sim 1.3$, and the lower panel to the downward wave packet, which has $k_y \sim -1.7$. Whistler wave packets with a given k_y evolve moving along the orbits at constant frequency. In Sim. 9 the frequency is $\omega_0 = 3$ that corresponds to an open orbit for the upper wave packet and to a closed orbit for the lower wave packet.

Fig. 6, middle panel, refers to Sim. 4 and shows the contour of b_x and the profiles of the soliton at time $t = 30$ (solid line) and $t = 0$ (dashed line). In this simulation, the lower wave packet has a wave vector k_y estimated to $k_y \sim -5$ (in agreement with the Fourier spectrum of the simulation results). The solution of the Hamiltonian equations for the wave packet with initial conditions $x(0) = 0, k_x(0) = 0$ gives wave packet reflected at nearly $\delta x \sim -1.5$ from the center of the soliton with $k_x \sim 25$ (in agreement with the small scales which form in the x direction at the edge of the soliton). In this point, the reflected frequency is estimated as $\omega_0' \sim \omega_0 - 2k_x V \sim 3.5$, which is below the minimum frequency calculated in correspondence to the edge of the soliton for $k_y \sim -5$, explaining why the lower wave packet does not propagate after reflection.

V. DISCUSSION AND CONCLUSIONS

In this paper, we have shown that whistler waves can be efficiently trapped and advected across the magnetic field lines by oblique magnetosonic slow solitons with typical scale length of the order or greater than the ion inertial length. Oblique slow solitons carry a quasi perpendicular density perturbation that is anti-correlated to the magnetic field perturbation, and since the propagation velocity of these solitons is much smaller than the phase velocity of whistlers, they can be viewed by whistlers as quasi stationary inhomogeneities. The soliton plasma density and magnetic field inhomogeneities then act as a true wave guide during whistler propagation. As a result, whistlers can be confined in correspondence to magnetic field depletions associated to density humps (magnetic holes), as we have shown for frequencies $\omega < \omega_{ce}/2$. Due to the presence of the magnetic field inhomogeneity, less strict conditions are required for trapping with respect to a channel provided by only a density variation. The possibility to advect whistlers marks an important difference with respect to the case where whistlers have been associated to non-propagating mirror modes. Numerical results based on a two-fluid model are in good agreement with theoretical expectations.

Slow solitons, acting as non-linear waves' carrier for whistlers, provide an efficient mechanism to confine whistler energy in space, thus avoiding the spreading of the wave packets, and to transport the whistler energy across magnetic field lines at the soliton typical speed. The model we propose is related to situations often encountered in space plasmas and could explain multi-point Cluster spacecraft observations in the Earth's magnetosphere. The mechanism of whistler trapping that we have discussed relies on the "inhomogeneous, slow nature" of the wave carrier, that is, the plasma density and magnetic field strength inhomogeneities are anti-correlated and quasi perpendicular to the background magnetic field and the velocity of propagation is smaller than the whistler phase velocity. We finally note that other solitonic structures, propagating slowly with respect to the whistler wave packet, could in principle play the same role in trapping and advecting the whistlers, thus explaining space observations often showing whistler waves in correspondence to local minimum or maximum of the large scale magnetic field and density, respectively. Moreover, this mechanism applies to any magnetic field configuration corresponding to a magnetic field depletion (with density hump), as long as the inhomogeneity is (quasi) perpendicular to the magnetic field. In addition to magnetosonic solitons and similar structures, the magnetic field associated to a current sheet, as it is found for instance in magnetic reconnection in the presence of a nonzero guide field, provides an important example of such configurations. This is of particular interest since it has been suggested that whistler waves are emitted during magnetic reconnection.[24] In this case, the channel provided by the inhomogeneity can in principle act as a guide for the emitted whistlers.

APPENDIX A: INITIAL CONDITIONS FOR SLOW MAGNETOSONIC SOLITONS

Below the initial conditions are given in the numerical code corresponding to a slow solitary wave.[22] Quantities are normalized to asymptotic equilibrium values outside the soliton

$$n_{sol} = \frac{A/\alpha}{\cos h^2[\sqrt{A/(12\mu)}x]}, \quad n = 1 + n_{sol},$$
$$P_{e,i} = P_{0e,i}(1 + \Gamma n_{sol}), \tag{A1}$$

$$B_x = \sin\varphi_0, \quad B_y = \cos\varphi_0 + \left[\frac{(v_{p0}^2 - c_s^2)}{\cos\varphi_0}\right]n_{sol}, \tag{A2}$$

$$B_z = -\frac{1}{v_{p0}}\frac{(d_e^{-2}-1)}{d_e^{-2}}\frac{v_{p0}^2(v_{p0}^2 - C_s^2)}{(v_{p0}^2 - \sin^2\varphi_0)}\frac{\sin\varphi_0}{\cos\varphi_0}$$
$$\times 2\sqrt{A/(12\mu)}\tan h[\sqrt{A/(12\mu)}x]n_{sol}, \tag{A3}$$

$$U_x = v_{p0}n_{sol}, \quad U_y = -\left[\frac{(v_{p0}^2 - c_s^2)}{v_{p0}}\right]\frac{\sin\varphi_0}{\cos\varphi_0}, \tag{A4}$$

$$U_z \sim u_{i,z} = -2\sqrt{A/(12\mu)}\frac{(v_{p0}^2 - c_s^2)(v_{p0}^2 d_e^2 - \sin\varphi_0^2)}{\cos\varphi_0(v_{p0}^2 - \sin\varphi_0^2)}$$
$$\times \tanh[\sqrt{A/(12\mu)}x]n_{sol}, \tag{A5}$$

where $c_s^2 = \Gamma(P_{e0} + P_{i0})$ is the sound speed in normalized units and

$$\mu = \frac{v_{p0}(v_{p0}^2 - c_s^2)}{4d_e^{-2}[v_{p0}^2 - (1+c_s^2)/2]}\left[1 - \frac{(d_e^{-2}-1)^2\sin^2\varphi_0}{d_e^{-2}(v_{p0}^2 - \sin^2\varphi_0)}\right], \tag{A6}$$

$$\alpha = \frac{3(v_{p0}^2 - c_s^2\sin^2\varphi_0) + (v_{p0}^2 - \sin^2\varphi_0)[c_s^2 + \Gamma^2(P_{e0} + P_{i0})]}{4v_{p0}[v_{p0}^2 - (1+c_s^2)/2]}, \tag{A7}$$

$$v_{p0}^2 = \frac{1}{2}\left[(1+c_s^2) - \sqrt{(1+c_s^2)^2 - 4c_s^2\sin^2\varphi_0}\right]. \tag{A8}$$

APPENDIX B: TWO-FLUID COLD DISPERSION RELATION

By linearizing the set of two fluid equations given by Eq. (14)–(19) in the cold limit $\omega/k \gg v_{th,e}$ ($v_{th,e}$ is the electron thermal speed), we get the following dispersion relation for whistler waves propagating in a homogeneous magnetized plasma at rest, at an angle θ with respect to the equilibrium magnetic field:

$$\omega^2 = \frac{1}{2}\frac{v_a^2 k^2}{(1+d_e^2 k^2)^2}\left\{(1+d_e^2 k^2)(1+\cos^2\theta) + \frac{k^2}{n}\cos^2\theta\right\}$$
$$+ \frac{1}{2}\frac{v_a^2 k^2}{(1+d_e^2 k^2)^2}\left\{\sqrt{(1+d_e^2 k^2)^2(1-\cos^2\theta)^2 + 2(1+d_e^2 k^2)\frac{k^2}{n}\cos^2\theta(1+\cos^2\theta) + \cos^4\theta\frac{k^4}{n^2}}\right\}. \tag{B1}$$

In Eq. (1), $v_a = B/\sqrt{n}$ is the Alfvén velocity in normalized units.

[1]E. J. Smith and B. T. Tsurutani, J. Geophys. Res. **81**(13), 2261, doi:10.1029/JA081i013p02261 (1976).

[2]R. M. Thorne and B. T. Tsurutani, Nature **293**, 384 (1981).

[3]B. T. Tsurutani and E. J. Smith, J. Geophys. Res. **87**(A8), 6060, doi:10.1029/JA087iA08p06060 (1982).

[4]W. Baumjohann, Ann. Geophys. **17**(12), 1528 (1999).

[5]E. M. Dubinin, Ann. Geophys. **25**(1), 303 (2007).

[6]R. L. Stenzel, J. Geophys. Res. **104**(A7), 14379, doi:10.1029/1998JA900120 (1999).

[7]E. J. Smith *et al.*, J. Geophys. Res. **65**(3), 815, doi:10.1029/JZ065i003p00815 (1960).

[8]V. I. Karpman and R. N. Kaufman, Sov. Phys. JETP **53**, 956 (1981).

[9]V. I. Karpman and R. N. Kaufman, J. Plasma Phys. **27**, 225 (1982).

[10]A. V. Streltsov *et al.*, J. Geophys. Res. **111**, A03216, doi:10.1029/2005JA011357 (2006).

[11]J. J. Angerami, J. Geophys. Res. **75**(31), 6115, doi:10.1029/JA075i031p06115 (1970).

[12]H. C. Koons, J. Geophys. Res. **94**(A11), 15393, doi:10.1029/JA094iA11p15393 (1989).

[13]O. A. Moullard, Geophys. Res. Lett. **29**(20), 1975, doi:10.1029/2002GL015101 (2002).

[14]R. L. Stenzel, Geophys. Res. Lett. **3**(2), 61, doi:10.1029/GL003i002p00061 (1976).

[15]J. F. McKenzie and T. B. Doyle, Phys. Plasmas **9**, 55 (2002).

[16]K. Stasiewicz *et al.*, Phys. Rev. Lett. **90**, 085002 (2003).

[17]K. Stasiewicz, Phys. Rev. Lett. **93**, 125004 (2004).

[18]K. Stasiewicz, J. Geophys. Res. **110**, A03220, doi:10.1029/2004JA010852 (2005).

[19]B. N. Breizman and A. V. Arefiev, Phys. Rev. Lett. **84**, 3863 (2000).

[20]T. H. Stix, *The Theory of Plasma Waves* (McGraw-Hill, New York, 1962).

[21]J. Heading, *An Introduction to Phase Integral Methods* (Methuen, 1962).

[22]Y. Ohsawa, Phys. Fluids **29**(6), 1844 (1986).

[23]F. Valentini *et al.*, J. Comput. Phys. **225**, 753 (2007).

[24]N. Singh, Phys. Rev. Lett. **107**, 245003 (2011).